Journal of Zhejiang University-SCIENCE C (Computers & Electronics)
ISSN 1869-1951 (Print); ISSN 1869-196X (Online)
www.zju.edu.cn/jzus; www.springerlink.com
E-mail: jzus@zju.edu.cn

Dynamic modeling of a 6-degree-of-freedom Stewart platform driven by a permanent magnet synchronous motor

Qiang MENG[†1], Tao ZHANG[1], Jing-feng HE[2], Jing-yan SONG[1], Jun-wei HAN[2]

([1]*Department of Automation, Tsinghua University, Beijing 100084, China*)

([2]*School of Mechatronic Engineering, Harbin Institute of Technology, Harbin 150001, China*)

[†]E-mail: meng-q09@mails.tsinghua.edu.cn

Received Nov. 18, 2009; Revision accepted Mar. 23, 2010; Crosschecked Aug. 31, 2010

Abstract: For an electrical six-degree-of-freedom Stewart platform, it is difficult to compute the equivalent inertia of each motor in real time, as the inertia is time-varying. In this study, an analysis using Kane's equation is undertaken of the driven torque of the movements of motor systems (including motor friction, movements of motor systems along with the actuators, rotation around axis of rotors and snails), as well as driven torque of the platform and actuators. The electromagnetic torque was calculated according to vector-controlled permanent magnet synchronous motor (PMSM) dynamics. By equalizing the driven torque and electromagnetic torque, a model was established. This method, taking into consideration the influence of counter electromotive force (EMF) and motor friction, could be applied to the real-time dynamic control of the platform, through which the calculation of the time-varying equivalent inertia is avoided. Finally, simulations with typically desired trajectory inputs are presented and the performance of the Stewart platform is determined. With this approach, the multi-body dynamics of the electrical Stewart platform is better understood.

Key words: Dynamics analysis, Six-degree-of-freedom Stewart platform, Kane's equation, Permanent magnet synchronous motor (PMSM), Vector control

doi:10.1631/jzus.C0910714 **Document code:** A **CLC number:** TP242.2

1 Introduction

The Gough-Stewart platform was first proposed by Gough (1956). In 1965, it was used as a 6-degree-of-freedom (6-DOF) motion platform for a flight simulator (Stewart, 1965). Since then, owing to its advantages of high rigidity, high accuracy, and high load-carrying capacity, the Stewart platform has been adopted in flight and vehicle simulators (Koekebakker, 2001), high-precision machining centers (Ting *et al*., 2004), force-torque sensors (Kang, 2001), and so forth.

In recent years, researchers have focused on the kinematics and dynamics of the Stewart platform (Shim *et al*., 1997; Yiu *et al*., 2001; Khalil and Guegan, 2004; Gao *et al*., 2005). Several methods, such as the Lagrange equation (Geng *et al*., 1992), the Newton-Euler equation (Dasgupta and Mruthyunjaya, 1998; Fu *et al*., 2007) and Kane's equation (Liu *et al*., 2000), have been proposed to derive the dynamic equations of the Stewart platform. Compared with the Newton-Euler method and Lagrange formulation, Kane's equation is more straightforward and systematic.

Two schemes are commonly applied in the control of the Stewart platform: task-space control (Kim and Lee, 1998; Liu *et al*., 2000) and joint-space control (Dasgupta and Choudhury, 1999; Omran *et al*., 2009). The first control scheme maps the joint space displacements to the task space through the direct kinematics, whose framework is multi-input multi-output (MIMO). The second scheme is developed by controlling each actuator of the platform as a single-input single-output (SISO) system. Consider-

ing the fact that the direct kinematics of the Stewart platform has no closed form or unique solution, the task-space control has some limitations in the experimental application.

Assuming the effect of actuators inertia was negligible, Fichter (1986) obtained a simple formula for computing the actuating forces for a Stewart platform. But as Ji (1993) pointed out, when the inertia of the load was not much larger than that of the actuators, the effect of actuators inertia is no longer negligible; thus, accurate modeling of dynamics including actuators is required. The electrical Stewart platform, however, contains two special movements: motor systems' movements with the actuators; rotors and snails' rotation around the axis. Few studies have mentioned these two movements before, and also, little published work exists on the electrical Stewart platform full dynamics, including actuation and control.

The permanent magnet synchronous motor (PMSM) has a great number of applications in industries, due to its compact structure, high power density, high torque/inertia ratio, and absence of rotor losses. Its performance, however, is very sensitive to parameter variations and external disturbances. To overcome the weakness, many control techniques such as sliding-mode control (Wai, 2001), robust proportional-integral-derivative (PID) control (Jan *et al.*, 2008), and neuro-fuzzy control (Elmas *et al.*, 2008) have been developed.

In the Stewart platform, the external load of PMSM is time-varying, which is generally concerned with the equivalent inertia of each motor. Because of the complexity of the Stewart platform, it is very difficult to compute the equivalent inertia in real time. Concerning the electrical 6-DOF Stewart platform, if one built the torque-force balance equation in motor dynamics, the time-varying equivalent inertia of each motor would have to be calculated in real time, or the model of the platform would not be precise.

To solve the problem of the equivalent inertia's calculation in real time, this paper deals with an improved multi-body dynamic model to calculate the required torque, and the building of PMSM dynamics to compute the electromagnetic torque, followed by the development of the precise, full dynamics of the platform. The original idea was that the torque-force balance equation is realized through only the Stewart platform dynamics, and the PMSM dynamic is not involved in the torque-force balance equation. We derive the dynamics of the Stewart platform based on Kane's equation. By changing the torque-force balance equation scheme, this method avoids the calculation of the time-varying equivalent inertia and can be used to analyze the performance of PMSM in the Stewart platform. This paper also deals with the analyses of the two special movements of the electrical Stewart platform and the calculation, through a numerical simulation, of their influence.

2 Mechanics of the Stewart platform

In this section, improved multi-body dynamics to compute the whole driven torque of the Stewart platform is built, including the movable platform, the actuators, and the motor systems.

The 6-DOF Stewart platform (Fig. 1) consists of a movable platform, a fixed base, and six extendable actuators.

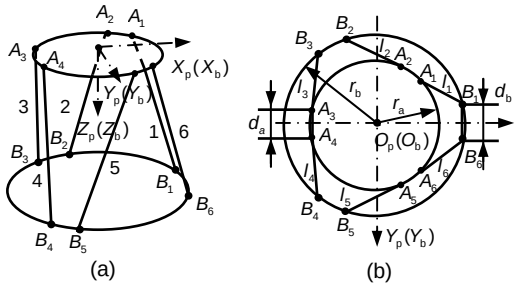

Fig. 1 Schematic view of a 6-DOF Stewart platform
(a) Side view; (b) Vertical view

To clearly describe the motion of the movable platform, we define a reference frame O_b-$X_bY_bZ_b$ fixed to the base and a platform frame O_p-$X_pY_pZ_p$ attached to the movable platform. $\boldsymbol{\chi}=[x, y, z, \varphi, \theta, \psi]^T$ is the vector of the movable platform generalized coordinates. Five parameters can describe the platform structure: upper joint radius r_a, lower joint radius r_b, upper joint spacing d_a, lower joint spacing d_b, and middle actuator length l_{i0}.

2.1 Kinematics analysis

The schematic view of a single actuator is shown in Fig. 2. Each actuator is driven by a corresponding motor, while the torque/force of the actuator is transmitted from synchronous belt and snail. Parameters subscript i represents the ith actuator.

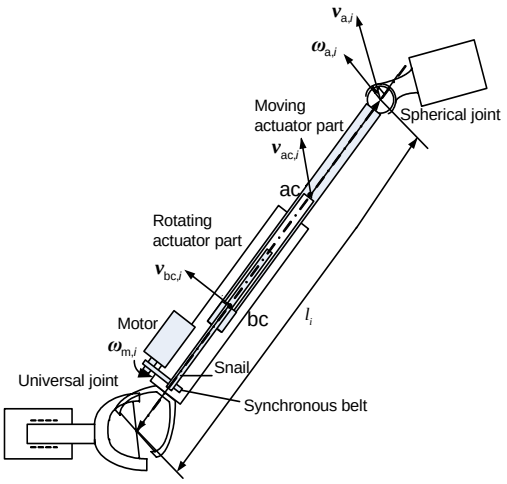

Fig. 2 Schematic view of a single actuator

Each actuator is driven by a corresponding motor, while the torque/force of the actuator is transmitted from synchronous belt and snail

The platform generalized velocity is defined as

$$\dot{\boldsymbol{q}} = \begin{bmatrix} \dot{\boldsymbol{t}}^{\mathrm{T}} & \boldsymbol{\omega}^{\mathrm{T}} \end{bmatrix}^{\mathrm{T}}, \tag{1}$$

where $\dot{\boldsymbol{t}}$ is the translation velocity of the platform, and $\boldsymbol{\omega}$ is the angular velocity of the platform.

The actuator vector $\boldsymbol{l}_i$ is given by

$$\boldsymbol{l}_i = \boldsymbol{t} + \boldsymbol{R}\boldsymbol{a}_i^{\mathrm{p}} - \boldsymbol{b}_i, \tag{2}$$

where $\boldsymbol{t}=[x, y, z]^{\mathrm{T}}$ is the translation vector of the platform, $\boldsymbol{a}_i^{\mathrm{p}}$ is the position vector of the upper joint in the platform frame, $\boldsymbol{b}_i$ is the position vector of the lower joint in the reference frame, and $\boldsymbol{R}$ is the rotation matrix.

The velocity of the upper joint $\boldsymbol{v}_{\mathrm{a},i}$ can be described by

$$\boldsymbol{v}_{\mathrm{a},i} = \dot{\boldsymbol{t}} + \boldsymbol{\omega} \times (\boldsymbol{R}\boldsymbol{a}_i^{\mathrm{p}}) = \boldsymbol{J}_{\boldsymbol{a}_i,\boldsymbol{q}} \dot{\boldsymbol{q}}, \tag{3}$$

where $\boldsymbol{J}_{\boldsymbol{a}_i,\boldsymbol{q}}$ is the Jacobian between the platform and the upper joint velocity.

Defining the transmission ratio between the rotor mechanical angular velocity $\boldsymbol{\omega}_{\mathrm{m},i}$ and the actuator linear velocity $\dot{\boldsymbol{l}}_i$ as $i_{\theta,l}$, the $\boldsymbol{\omega}_{\mathrm{m},i}$ can be described by

$$\boldsymbol{\omega}_{\mathrm{m},i} = i_{\theta,l}\dot{\boldsymbol{l}}_i = i_{\theta,l}\left(\boldsymbol{l}_{\mathrm{n},i}^{\mathrm{T}}\dot{\boldsymbol{t}} + \boldsymbol{l}_{\mathrm{n},i}^{\mathrm{T}}(\boldsymbol{\omega} \times (\boldsymbol{R}\boldsymbol{a}_i^{\mathrm{p}}))\right) = \boldsymbol{J}_{\boldsymbol{\theta}_i,\boldsymbol{q}}\dot{\boldsymbol{q}}, \tag{4}$$

where $\boldsymbol{l}_{\mathrm{n},i}=\boldsymbol{l}_i/\|\boldsymbol{l}_i\|$, and $\boldsymbol{J}_{\boldsymbol{\theta}_i,\boldsymbol{q}}$ is the Jacobian between the platform velocity and the rotor angular velocity.

The rotor mechanical angular acceleration $\boldsymbol{a}_{\mathrm{m},i}$ can be written as

$$\begin{aligned} \boldsymbol{a}_{\mathrm{m},i} &= i_{\theta,l}(\boldsymbol{l}_{\mathrm{n},i}^{\mathrm{T}}\dot{\boldsymbol{v}}_{\mathrm{a},i} + \dot{\boldsymbol{l}}_{\mathrm{n},i}^{\mathrm{T}}\boldsymbol{v}_{\mathrm{a},i}) \\ &= i_{\theta,l}\boldsymbol{l}_{\mathrm{n},i}^{\mathrm{T}}\dot{\boldsymbol{v}}_{\mathrm{a},i} + i_{\theta,l}\boldsymbol{v}_{\mathrm{a},i}^{\mathrm{T}}\left(\frac{1}{\|\boldsymbol{l}_i\|}\boldsymbol{P}_{l\mathrm{n}}\right)\boldsymbol{v}_{\mathrm{a},i}, \end{aligned} \tag{5}$$

where $\boldsymbol{P}_{l\mathrm{n}}$ is the projector to the (hyper)plane with normal vector $\boldsymbol{l}_{\mathrm{n},i}$.

The actuator angular velocity is given by

$$\boldsymbol{\omega}_{\mathrm{a},i} = \boldsymbol{l}_{\mathrm{n},i} \times \frac{\boldsymbol{v}_{\mathrm{a},i}}{\|\boldsymbol{l}_i\|}. \tag{6}$$

Defining the mass center of the moving actuator part and the rotating part as ac and bc, respectively, thus their velocities and acceleration can be described as

$$\begin{cases} \boldsymbol{v}_{\mathrm{ac},i} = \boldsymbol{v}_{\mathrm{a},i} + \boldsymbol{\omega}_{\mathrm{a},i} \times (-r_{\mathrm{ac}}\boldsymbol{l}_{\mathrm{n},i}) = \boldsymbol{J}_{\mathrm{ac,a},i}\boldsymbol{v}_{\mathrm{a},i}, \\ \dot{\boldsymbol{v}}_{\mathrm{ac},i} = \dot{\boldsymbol{J}}_{\mathrm{ac,a},i}\boldsymbol{v}_{\mathrm{a},i} + \boldsymbol{J}_{\mathrm{ac,a},i}\dot{\boldsymbol{v}}_{\mathrm{a},i}, \\ \boldsymbol{v}_{\mathrm{bc},i} = \boldsymbol{\omega}_{\mathrm{a},i} \times (r_{\mathrm{bc}}\boldsymbol{l}_{\mathrm{n},i}) = \boldsymbol{J}_{\mathrm{bc,a},i}\boldsymbol{v}_{\mathrm{a},i}, \\ \dot{\boldsymbol{v}}_{\mathrm{bc},i} = \dot{\boldsymbol{J}}_{\mathrm{bc,a},i}\boldsymbol{v}_{\mathrm{a},i} + \boldsymbol{J}_{\mathrm{bc,a},i}\dot{\boldsymbol{v}}_{\mathrm{a},i}, \end{cases} \tag{7}$$

where r_{ac} is the distance from point ac to the upper joint, r_{bc} is the distance from point bc to the lower joint, $\boldsymbol{J}_{\mathrm{bc,a},i}$ is the Jacobian between the upper joint and the moving actuator part velocity, and $\boldsymbol{J}_{\mathrm{bc,a},i}$ is the Jacobian between the upper joint and the rotating actuator part velocity.

The acceleration of the upper joint can be described by differentiating Eq. (3):

$$\begin{aligned} \dot{\boldsymbol{v}}_{\mathrm{a}i} &= \ddot{\boldsymbol{t}} + \dot{\boldsymbol{\omega}} \times (\boldsymbol{R}\boldsymbol{a}_i^{\mathrm{p}}) + \boldsymbol{\omega} \times (\boldsymbol{\omega} \times (\boldsymbol{R}\boldsymbol{a}_i^{\mathrm{p}})) \\ &= \boldsymbol{J}_{\boldsymbol{a}_i,\boldsymbol{q}}\ddot{\boldsymbol{q}} - \|\boldsymbol{\omega}\|^2 \boldsymbol{P}_{\boldsymbol{\omega}}\boldsymbol{a}_i^{\mathrm{p}}, \end{aligned} \tag{8}$$

where $\boldsymbol{P}_{\boldsymbol{\omega}} = \boldsymbol{I} - \boldsymbol{\omega}_{\mathrm{n}}\boldsymbol{\omega}_{\mathrm{n}}^{\mathrm{T}}$.

2.2 Multi-body dynamics analysis

2.2.1 Movable platform dynamics

Based on analyzing the movable platform, the dynamics of the platform is governed by

$$\begin{bmatrix} K_{\mathrm{F,T}}\boldsymbol{L}_{\mathrm{n}} \\ K_{\mathrm{F,T}}\boldsymbol{R}\boldsymbol{A}^{\mathrm{p}}\times\boldsymbol{L}_{\mathrm{n}} \end{bmatrix}\boldsymbol{T}_{\mathrm{a}} = \begin{bmatrix} m_{\mathrm{p}}\boldsymbol{I} & \boldsymbol{0} \\ \boldsymbol{0} & \boldsymbol{I}_{\mathrm{p}} \end{bmatrix}\begin{bmatrix} \ddot{\boldsymbol{t}} \\ \dot{\boldsymbol{\omega}} \end{bmatrix} + \begin{bmatrix} \boldsymbol{0} & \boldsymbol{0} \\ \boldsymbol{0} & \tilde{\boldsymbol{\omega}}\boldsymbol{I}_{\mathrm{p}} \end{bmatrix}\begin{bmatrix} \dot{\boldsymbol{t}} \\ \boldsymbol{\omega} \end{bmatrix} - \begin{bmatrix} m_{\mathrm{p}}\boldsymbol{g} \\ \boldsymbol{0} \end{bmatrix}. \tag{9}$$

In short,

$$\eta\boldsymbol{J}_{\theta,\boldsymbol{q}}^{\mathrm{T}}(\boldsymbol{\chi})\boldsymbol{T}_{\mathrm{a}} = \boldsymbol{M}_{\mathrm{p}}(\boldsymbol{\chi})\ddot{\boldsymbol{q}} + \boldsymbol{C}_{\mathrm{p}}(\boldsymbol{\chi},\dot{\boldsymbol{q}})\dot{\boldsymbol{q}} + \boldsymbol{G}_{\mathrm{p}}(\boldsymbol{\chi}). \tag{10}$$

Herein $\boldsymbol{T}_{\mathrm{a}}$ is the motor electromagnetic torque matrix; $\boldsymbol{J}_{\theta\boldsymbol{q}}(\boldsymbol{\chi})$, $\boldsymbol{L}_{\mathrm{n}}$, and $\boldsymbol{A}^{\mathrm{p}}$ are the matrices consisting of $\boldsymbol{J}_{\boldsymbol{\theta}_i,\boldsymbol{q}}$, $\boldsymbol{l}_{\mathrm{n},i}$, and $\boldsymbol{a}_i^{\mathrm{p}}$, respectively; $K_{\mathrm{F,T}}$ is the force-torque conversion coefficient between the actuator force and the motor torque; m_{p} is the mass of the platform; $\tilde{\boldsymbol{\omega}}$ is a skew-symmetric matrix representing operator $\boldsymbol{\omega}$; $\boldsymbol{I}_{\mathrm{p}} = \boldsymbol{R}\boldsymbol{I}_{\mathrm{p}}^{\mathrm{p}}\boldsymbol{R}^{\mathrm{T}}$, where $\boldsymbol{I}_{\mathrm{p}}^{\mathrm{p}}$ is the inertia matrix of the platform in the platform frame; $\eta=K_{\mathrm{F,T}}/i_{\theta,l}$ is the transfer efficiency; $\boldsymbol{M}_{\mathrm{p}}(\boldsymbol{\chi})$ denotes the mass matrix of the movable platform; $\boldsymbol{C}_{\mathrm{p}}(\boldsymbol{\chi},\dot{\boldsymbol{q}})$ contains the Coriolis and centripetal terms of the movable platform; $\boldsymbol{G}_{\mathrm{p}}(\boldsymbol{\chi})$ represents the gravitational effects of the movable platform.

2.2.2 Influence of the actuator inertial forces

In the dynamics modeling, the gimbals are assumed to rotate frictionlessly, and the inertia of both actuator parts rotating around the actuator direction is neglected. Therefore, the mass properties of each actuator part can be described by two parameters, the mass and the inertia around an axis orthogonal to the actuator direction. Mass m_{a} and inertia i_{a} are taken for the moving part of the actuator, and (m_{b}, i_{b}) for the rotating part.

The inertial force generated by the movement of the moving actuator part is described at the upper joint as

$$\begin{cases} \boldsymbol{f}_{\mathrm{ma},i}^{\mathrm{a}} = \boldsymbol{J}_{\mathrm{ac,a},i}^{\mathrm{T}} m_{\mathrm{a}}\dot{\boldsymbol{v}}_{\mathrm{ac},i} = \boldsymbol{J}_{\mathrm{ac,a},i}^{\mathrm{T}} m_{\mathrm{a}}(\boldsymbol{J}_{\mathrm{ac,a},i}\dot{\boldsymbol{v}}_{\mathrm{a},i} + \dot{\boldsymbol{J}}_{\mathrm{ac,a},i}\boldsymbol{v}_{\mathrm{a},i}) \\ \qquad = \boldsymbol{M}_{\mathrm{ma},i}\dot{\boldsymbol{v}}_{\mathrm{a},i} + \boldsymbol{C}_{\mathrm{ma},i}\boldsymbol{v}_{\mathrm{a},i}, \\ \boldsymbol{M}_{\mathrm{ma},i} = \boldsymbol{J}_{\mathrm{ac,a},i}^{\mathrm{T}} m_{\mathrm{a}}\boldsymbol{J}_{\mathrm{ac,a},i}, \quad \boldsymbol{C}_{\mathrm{ma},i} = \boldsymbol{J}_{\mathrm{ac,a},i}^{\mathrm{T}} m_{\mathrm{a}}\dot{\boldsymbol{J}}_{\mathrm{ac,a},i}. \end{cases} \tag{11}$$

The gravitational forces of the moving actuator part and the rotating actuator part can be described at the upper joint as

$$\boldsymbol{G}_{\mathrm{a},i}^{\mathrm{a}} = \boldsymbol{J}_{\mathrm{ac,a},i}^{\mathrm{T}} m_{\mathrm{a}}\boldsymbol{g}, \tag{12}$$

$$\boldsymbol{G}_{\mathrm{b},i}^{\mathrm{a}} = \boldsymbol{J}_{\mathrm{bc,a},i}^{\mathrm{T}} m_{\mathrm{b}}\boldsymbol{g}. \tag{13}$$

The inertial forces generated by the inertias of the moving actuator part and the rotating actuator part can be taken together. Defining $\boldsymbol{p}_{\mathrm{a}}$ as the position vector of the upper joint, the inertial forces can be described at the upper joint (Koekebakker, 2001):

$$\boldsymbol{f}_{\mathrm{ia,ib},i}^{\mathrm{a}} = \boldsymbol{M}_{\mathrm{ia,ib},i}\dot{\boldsymbol{v}}_{\mathrm{a},i} + \boldsymbol{C}_{\mathrm{ia,ib},i}\boldsymbol{v}_{\mathrm{a},i}. \tag{14}$$

2.2.3 Influence of motor systems' mechanical movements

Rotor and snail are rotating around their axes while the motor system is moving with the rotating actuator part. For the first movement, we define their total inertia in the motor frame as i_{R}; for the second movement, we define their mass and translational inertia (including the motor and snail) as m_{s}, i_{s}.

The inertial force generated by the rotation of rotor and snail can be described at the motor axis:

$$\begin{aligned} \boldsymbol{T}_{\mathrm{R},i}^{\theta} &= i_{\mathrm{R}}\boldsymbol{a}_{\mathrm{m},i} = i_{\mathrm{R}}i_{\theta,l}\boldsymbol{l}_{\mathrm{n},i}^{\mathrm{T}}\dot{\boldsymbol{v}}_{\mathrm{a},i} + i_{\mathrm{R}}i_{\theta,l}\boldsymbol{v}_{\mathrm{a},i}^{\mathrm{T}}\left(\frac{1}{\|\boldsymbol{l}_i\|}\boldsymbol{P}_{l\mathrm{n}}\right)\boldsymbol{v}_{\mathrm{a},i} \\ &= \boldsymbol{M}_{\mathrm{TR},i}\dot{\boldsymbol{v}}_{\mathrm{a},i} + \boldsymbol{C}_{\mathrm{TR},i}\boldsymbol{v}_{\mathrm{a},i}. \end{aligned} \tag{15}$$

The motor friction can be given by

$$\boldsymbol{f}_{\mathrm{f},i}^{\theta} = B_{\mathrm{m}}\boldsymbol{\omega}_{\mathrm{m},i}, \tag{16}$$

where B_{m} is the viscous friction coefficient.

$\boldsymbol{T}_{\mathrm{R}}^{\theta}$ and $\boldsymbol{f}_{\mathrm{f},i}^{\theta}$ can be projected onto the platform generalized coordinates, resulting in

$$\begin{cases} \boldsymbol{f}_{\mathrm{TR},i} = \boldsymbol{J}_{\boldsymbol{\theta}_i,\boldsymbol{q}}^{\mathrm{T}}\boldsymbol{T}_{\mathrm{R},i}^{\theta} = \boldsymbol{J}_{\boldsymbol{\theta}_i,\boldsymbol{q}}^{\mathrm{T}}\boldsymbol{M}_{\mathrm{TR},i}\dot{\boldsymbol{v}}_{\mathrm{a},i} + \boldsymbol{J}_{\boldsymbol{\theta}_i,\boldsymbol{q}}^{\mathrm{T}}\boldsymbol{C}_{\mathrm{TR},i}\boldsymbol{v}_{\mathrm{a},i}, \\ \boldsymbol{f}_{\mathrm{f},i} = \boldsymbol{J}_{\boldsymbol{\theta}_i,\boldsymbol{q}}^{\mathrm{T}}\boldsymbol{f}_{\mathrm{f},i}^{\theta} = \boldsymbol{J}_{\boldsymbol{\theta}_i,\boldsymbol{q}}^{\mathrm{T}}B_{\mathrm{m}}\boldsymbol{J}_{\boldsymbol{\theta}_i,\boldsymbol{q}}\dot{\boldsymbol{q}}. \end{cases} \tag{17}$$

Using Eqs. (13) and (14), the inertial forces generated by the movement of the motor system can be described at the upper joint as

$$\boldsymbol{G}_{\mathrm{ms},i}^{\mathrm{a}} = \boldsymbol{J}_{\mathrm{bc,a},i}^{\mathrm{T}} m_{\mathrm{s}}\boldsymbol{g}, \tag{18}$$

$$\begin{aligned}\boldsymbol{f}_{\mathrm{is},i}^{\mathrm{a}} &= \frac{i_{\mathrm{s}}}{i_{\mathrm{a}}+i_{\mathrm{b}}}(\boldsymbol{M}_{\mathrm{ia,ib},i}\dot{\boldsymbol{v}}_{\mathrm{a},i}+\boldsymbol{C}_{\mathrm{ia,ib},i}\boldsymbol{v}_{\mathrm{a},i})\\ &= \boldsymbol{M}_{\mathrm{is},i}\dot{\boldsymbol{v}}_{\mathrm{a},i}+\boldsymbol{C}_{\mathrm{is},i}\boldsymbol{v}_{\mathrm{a},i}.\end{aligned} \tag{19}$$

2.2.4 Stewart platform dynamics

The total inertial forces generated by the actuators and the motor systems can be described at the platform coordinates as

$$\begin{aligned}\boldsymbol{f}_{\mathrm{g}}^{*} = \sum_{i=1}^{6}\boldsymbol{J}_{\boldsymbol{a}_i,\boldsymbol{q}}^{\mathrm{T}}(&\boldsymbol{f}_{\mathrm{ma},i}^{\mathrm{a}}+\boldsymbol{f}_{\mathrm{ia,ib},i}^{\mathrm{a}}+\boldsymbol{G}_{\mathrm{a},i}^{\mathrm{a}}+\boldsymbol{G}_{\mathrm{b},i}^{\mathrm{a}}\\ &+\boldsymbol{G}_{\mathrm{ms},i}^{\mathrm{a}}+\boldsymbol{f}_{\mathrm{is},i}^{\mathrm{a}})+\sum_{i=1}^{6}(\boldsymbol{f}_{\mathrm{TR},i}+\boldsymbol{f}_{\mathrm{f},i}).\end{aligned} \tag{20}$$

Combing Eq. (10), the total inertial forces of the Stewart platform are

$$\boldsymbol{f}^{*} = \boldsymbol{f}_{\mathrm{g}}^{*}+\boldsymbol{M}_{\mathrm{p}}(\boldsymbol{\chi})\ddot{\boldsymbol{q}}+\boldsymbol{C}_{\mathrm{p}}(\boldsymbol{\chi},\dot{\boldsymbol{q}})\dot{\boldsymbol{q}}+\boldsymbol{G}_{\mathrm{p}}(\boldsymbol{\chi}). \tag{21}$$

On the other hand, the active forces can be given by

$$\boldsymbol{f} = \eta\boldsymbol{J}_{\theta,\boldsymbol{q}}^{\mathrm{T}}\boldsymbol{T}_{\mathrm{a}}. \tag{22}$$

Using Kane's method, the Stewart platform dynamics can be written as

$$\begin{cases}\eta\boldsymbol{J}_{\theta,\boldsymbol{q}}^{\mathrm{T}}\boldsymbol{T}_{\mathrm{a}} = \boldsymbol{M}_{\mathrm{s}}(\boldsymbol{\chi})\ddot{\boldsymbol{q}}+\boldsymbol{C}_{\mathrm{s}}(\boldsymbol{\chi},\dot{\boldsymbol{q}})+\boldsymbol{G}_{\mathrm{s}}(\boldsymbol{\chi}),\\ \boldsymbol{M}_{\mathrm{s}}(\boldsymbol{\chi}) = \boldsymbol{M}_{\mathrm{p}}(\boldsymbol{\chi})+\sum_{i=1}^{6}\boldsymbol{J}_{\theta_i,\boldsymbol{q}}^{\mathrm{T}}\boldsymbol{M}_{\mathrm{TR},i}J_{\boldsymbol{a}_i,\boldsymbol{q}}\\ \qquad +\sum_{i=1}^{6}\Big(\boldsymbol{J}_{\boldsymbol{a}_i,\boldsymbol{q}}^{\mathrm{T}}(\boldsymbol{M}_{\mathrm{ma},i}+\boldsymbol{M}_{\mathrm{ia,ib},i}+\boldsymbol{M}_{\mathrm{is},i})\Big)\boldsymbol{J}_{\boldsymbol{a}_i,\boldsymbol{q}},\\ \boldsymbol{C}_{\mathrm{s}}(\boldsymbol{\chi},\dot{\boldsymbol{q}}) = \sum_{i=1}^{6}\Big(\boldsymbol{J}_{\boldsymbol{a}_i,\boldsymbol{q}}^{\mathrm{T}}(\boldsymbol{C}_{\mathrm{ma},i}+\boldsymbol{C}_{\mathrm{ia,ib},i}+\boldsymbol{C}_{\mathrm{is},i})\boldsymbol{J}_{\boldsymbol{a}_i,\boldsymbol{q}}\dot{\boldsymbol{q}}\\ \qquad +\boldsymbol{J}_{\theta_i,\boldsymbol{q}}^{\mathrm{T}}(\boldsymbol{C}_{\mathrm{TR},i}\boldsymbol{J}_{\boldsymbol{a}_i,\boldsymbol{q}}+\boldsymbol{B}_{\mathrm{m}}\boldsymbol{J}_{\theta_i,\boldsymbol{q}})\dot{\boldsymbol{q}}\\ \qquad -\|\boldsymbol{\omega}\|^2\boldsymbol{J}_{\boldsymbol{a}_i,\boldsymbol{q}}^{\mathrm{T}}(\boldsymbol{M}_{\mathrm{ma},i}+\boldsymbol{M}_{\mathrm{ia,ib},i}+\boldsymbol{M}_{\mathrm{is},i})\boldsymbol{P}_{\boldsymbol{\omega}}\boldsymbol{a}_i^{\mathrm{p}}\\ \qquad -\|\boldsymbol{\omega}\|^2\boldsymbol{J}_{\theta_i,\boldsymbol{q}}^{\mathrm{T}}\boldsymbol{M}_{\mathrm{TR},i}\boldsymbol{P}_{\boldsymbol{\omega}}\boldsymbol{a}_i^{\mathrm{p}}\Big)+\boldsymbol{C}_{\mathrm{p}}(\boldsymbol{\chi},\dot{\boldsymbol{q}})\dot{\boldsymbol{q}},\\ \boldsymbol{G}_{\mathrm{s}}(\boldsymbol{\chi}) = \boldsymbol{G}_{\mathrm{p}}(\boldsymbol{\chi})+\sum_{i=1}^{6}\boldsymbol{J}_{\boldsymbol{a}_i,\boldsymbol{q}}^{\mathrm{T}}(\boldsymbol{G}_{\mathrm{a},i}^{\mathrm{a}}+\boldsymbol{G}_{\mathrm{b},i}^{\mathrm{a}}+\boldsymbol{G}_{\mathrm{ms},i}^{\mathrm{a}}),\end{cases} \tag{23}$$

where $\boldsymbol{M}_{\mathrm{s}}(\boldsymbol{\chi})$ is the mass matrix of the Stewart platform, $\boldsymbol{C}_{\mathrm{s}}(\boldsymbol{\chi},\dot{\boldsymbol{q}})$ contains the Coriolis and centripetal terms of the Stewart platform, and $\boldsymbol{G}_{\mathrm{s}}(\boldsymbol{\chi})$ represents the gravitational effects of the Stewart platform.

3 PMSM driven mechanical system model

The PMSM driven system (Fig. 3) consists of a speed controller, a reference current regulator, a hysteresis band current controller and a three phase pulse width modulation (PWM) inverter.

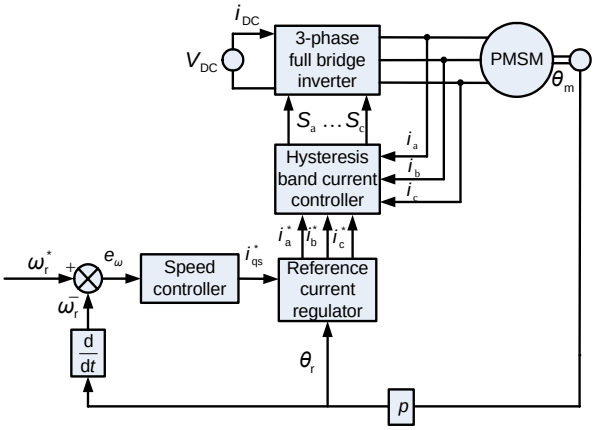

Fig. 3 Block diagram of the speed control of a permanent magnet synchronous motor (PMSM) drive

V_{DC} is the DC link voltage; i_{DC} is the DC link current; θ_m is the rotor mechanical position; i_a^*, i_b^*, i_c^* are the reference phase currents; i_a, i_b, i_c are the actual phase currents; ω_r^* is the reference speed; ω_r is the actual speed; the speed controller generates control current by using speed error e_ω

The typical model of a PMSM in the synchronous rotor-rotating reference frame (dq) can be described as (Chen, 2006)

$$u_{\mathrm{ds}} = R_{\mathrm{s}}i_{\mathrm{ds}}+L_{\mathrm{d}}pi_{\mathrm{ds}}-\omega_{\mathrm{r}}L_{\mathrm{q}}i_{\mathrm{qs}}, \tag{24}$$

$$u_{\mathrm{qs}} = R_{\mathrm{s}}i_{\mathrm{qs}}+L_{\mathrm{q}}pi_{\mathrm{qs}}+\omega_{\mathrm{r}}L_{\mathrm{d}}i_{\mathrm{ds}}+\omega_{\mathrm{r}}\psi_{\mathrm{r}}, \tag{25}$$

$$T_{\mathrm{a}} = P\left[\psi_{\mathrm{r}}i_{\mathrm{qs}}+(L_{\mathrm{d}}-L_{\mathrm{q}})i_{\mathrm{ds}}i_{\mathrm{qs}}\right], \tag{26}$$

where (i_{ds}, i_{qs}), (L_d, L_q), and (u_{ds}, u_{qs}) represent stator currents, stator inductance, and voltages in the rotor-rotating frame (dq) respectively, T_a is the electromagnetic torque, R_s is the stator resistance, ψ_f is the stator fluxes, p is the differential operator, P is the number of pole-pairs, and ω_r is the actual speed.

Through realizing i_{ds}=0 by applying field-oriented control, the model of PMSM can be rewritten as

$$u_{ds} = -\omega_r L_q i_{qs}, \tag{27}$$

$$u_{qs} = R_s i_{qs} + L_q p i_{qs} + e_0, \tag{28}$$

$$e_0 = \omega_r \psi_r, \tag{29}$$

$$T_a = P\psi_r i_{qs} = K_m i_{qs}, \tag{30}$$

where e_0 is the back electromotive force (EMF), $K_m=P\psi_f$.

Considering the parameter variations, the electromechanical equation of the PMSM is

$$\tilde{J}_m \frac{d\omega_m}{dt} + B_m\omega_m = T_a - T_l, \tag{31}$$

$$\omega_r = P\omega_m, \tag{32}$$

where $\tilde{J}_m$ is the uncertain inertia, B_m is the viscous friction coefficient, T_1 is the load torque, and ω_m is the rotor mechanical velocity.

The simplified block diagram of the field-oriented controlled PMSM driven system is shown in Fig. 4.

4 PMSM driven Stewart platform

4.1 Integrated system

We need to solve two problems for modeling the full Stewart platform dynamics.

Problem 1 It is difficult to compute the time-varying parameter $\tilde{J}_m$ in real time.

As far as the electrical Stewart platform is concerned, its torque-force balance equation is generally built by motor dynamics, such as Eq. (31); hence, we encounter and must deal with this problem. Due to the highly nonlinear, strong coupling and parameters variations of the Stewart platform, it becomes impossible to compute $\tilde{J}_m$ in real time.

By realizing the torque-force balance equation through the Stewart platform dynamics, we change the modeling strategies. In detail, except for the movements of the movable platform and actuators, the movements of motor systems, including the motor friction, rotors and snails' rotation around the axis, and motor systems' movements with the actuators, are also analyzed using Kane's equation. PMSM dynamics is used to calculate only the electromagnetic torque.

Problem 2 For an electrical Stewart platform, how to analyze the influence of back EMF?

In the Stewart platform dynamics, the actual rotor position and speed are calculated, and then fed back to the PMSM dynamics; thus, the full Stewart platform dynamics are developed.

The back EMF e_0 is in direct proportion to ω_r, and ω_r has been computed using the Stewart platform dynamics.

Finally, the full Stewart platform dynamics are shown in Fig. 5.

4.2 Controller design

In the analog control system, the most popular controller is the PID controller, which is a linear controller. According to the given value $r_{in}(t)$ and the actual output value $y_{out}(t)$, we constitute the control error

$$\text{error}(t) = r_{in}(t) - y_{out}(t). \tag{33}$$

The PID control law is

$$u(t) = K_p\text{error}(t) + K_I\int \text{error}(t)dt + K_D\frac{d}{dt}\text{error}(t), \tag{34}$$

where K_P, K_I, and K_D are the proportional, integral, and differential coefficients, respectively.

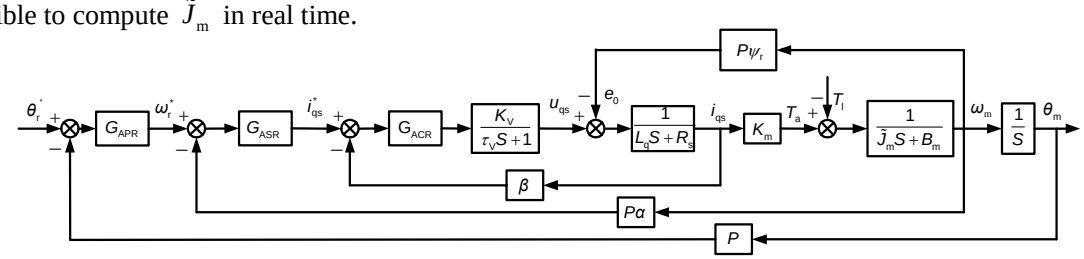

Fig. 4 Simplified control block diagram of the field-oriented controlled PMSM driven system

G_{APR}, G_{ASR}, and G_{ACR} are the position loop, speed loop, and currents loop controllers, respectively; $K_V/(\tau_V S+1)$ is the simplified transfer function of the PWM inverter (Chen *et al*., 2004); K_V is the inverter magnification ratio; τ_V is the inverter delay time constant; α and β are the speed and current feedback coefficient, respectively

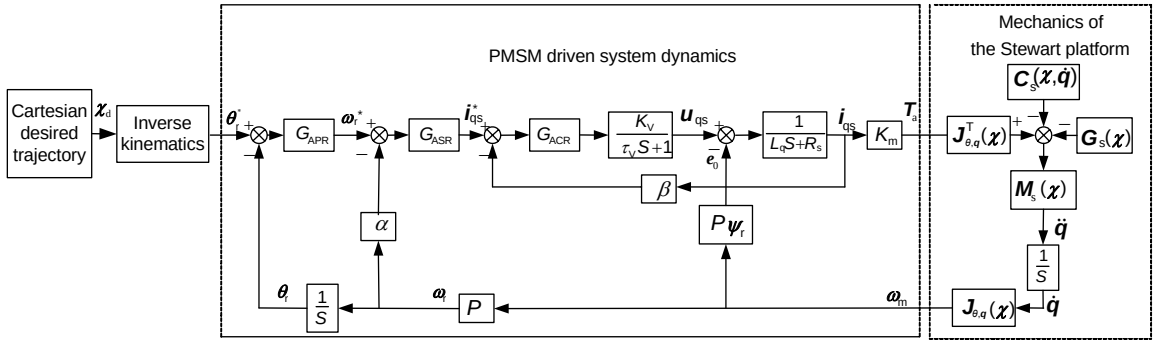

Fig. 5 Full dynamics of the Stewart platform driven by a permanent magnet synchronous motor (PMSM)

In Fig. 5, all of the controllers G_{APR}, G_{ASR}, and G_{ACR} are PID controllers. The controller parameters are designed in accordance with the engineering design method of Chen (2006), and can be fine-tuned according to experience.

5 Simulation

Consider a real application, whose main parameters of the Stewart platform are shown in Tables 1–4.

Since the characteristics of the 6 DOFs of the Stewart platform are different, it is difficult to achieve the optimization simultaneously for them. By optimizing the controller parameters, the available frequency response curve is as shown in Fig. 6, which can be calculated using the 'linear analysis' tools in Matlab.

Table 1 Structure parameters of the platform

Parameter	Value (m)
Upper joint radius, r_a	0.8
Lower joint radius, r_b	1.1
Upper joint spacing, d_a	0.2
Lower joint spacing, d_b	0.3
Middle actuator length, l_{i0}	1.86

Table 2 Parameters of the permanent magnet synchronous motor (PMSM)

Parameter	Value
Power	5150 W
Rated speed, ω_n	314 rad/s
Rated current, I_n	13.4 A
Number of pairs, P	4
Torque constant, K_m	1.5 N·m/A
Stator inductance, L_q	6.9 M·h
Stator resistance, R_s	0.7 Ω
Viscous friction coefficient, B_m	0.007 92 N·s/rad
Inverter magnification ratio, K_V	50.7 V/A

Table 3 Parameters of the load and conversion coefficient

Parameter	Value
Platform mass, m_p	950 kg
Actuator's moving part mass, m_a	30 kg
Actuator's rotating part mass, m_b	50 kg
Rotor and snail mass, m_s	27.6 kg
Rotor and snail inertia, i_R	6.66×10^{-3} kg/m^2
Force-torque conversion coefficient, $K_{F,T}$	250 N/(N·m)

Table 4 Limit conditions of the Stewart platform

Parameter	Value
Actuator length, l_i	1.535–2.2 m
Peak speed, ω_{max}	600 rad/s
Peak current, I_{max}	42 A

In Fig. 6a, the −3 dB point can be found at 14–15 Hz for the directions of surge (χ_1), sway (χ_2), and yaw (χ_6), whereas the bandwidths are lower for the directions of roll (χ_4), pitch (χ_5), and heave (χ_3), which are about 11−12 Hz. Put simply, all the bandwidths of the 6 DOFs are above 10 Hz; thus, the platform has a satisfactory dynamic response.

In Fig. 6b, the frequency response curve of surge has a resonance peak, so its adjustment time is the longest and position tracking ability is the worst. Therefore, the surge is taken as an example to analyze the position and orientation tracking performance of the Stewart platform.

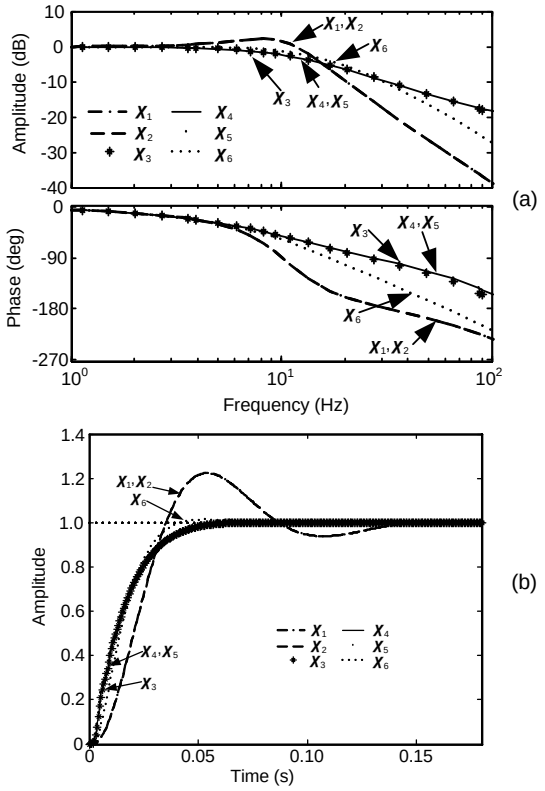

Fig. 6 Frequency response of the Stewart platform
(a) Bode plot; (b) Step response

The Cartesian desired trajectories of the platform are assumed to be

$$\begin{cases} \text{Surge}: \chi_1 = 0.1\sin(2\pi\times 0.2t)\ \text{m}, \\ \text{Sway}: \chi_2 = 0.2\sin(2\pi\times 0.2t)\ \text{m}, \\ \text{Heave}: \chi_3 = 0.3\sin(2\pi\times 0.2t)\ \text{m}, \\ \text{Roll}: \chi_4 = 5^\circ\sin(2\pi\times 0.3t), \\ \text{Pitch}: \chi_5 = 10^\circ\sin(2\pi\times 0.3t), \\ \text{Yaw}: \chi_6 = 15^\circ\sin(2\pi\times 0.3t). \end{cases} \tag{35}$$

Assuming an external impact load is forced on the movable platform, its formula at the platform coordinates can be written as

$$\begin{cases} \boldsymbol{F}_{\text{ext}} = (0,0,F_{\text{z\_ext}},0,0,0), \\ F_{\text{z\_ext}} = \begin{cases} 500\ \text{N}, & 2.5 \le t \le 2.52, \\ 0\ \text{N}, & \text{otherwise}. \end{cases} \end{cases} \tag{36}$$

With the proposed model, we can obtain the curves of position tracking (Fig. 7), motor speed (Fig. 8a), and the electromagnetic torque (Fig. 8b).

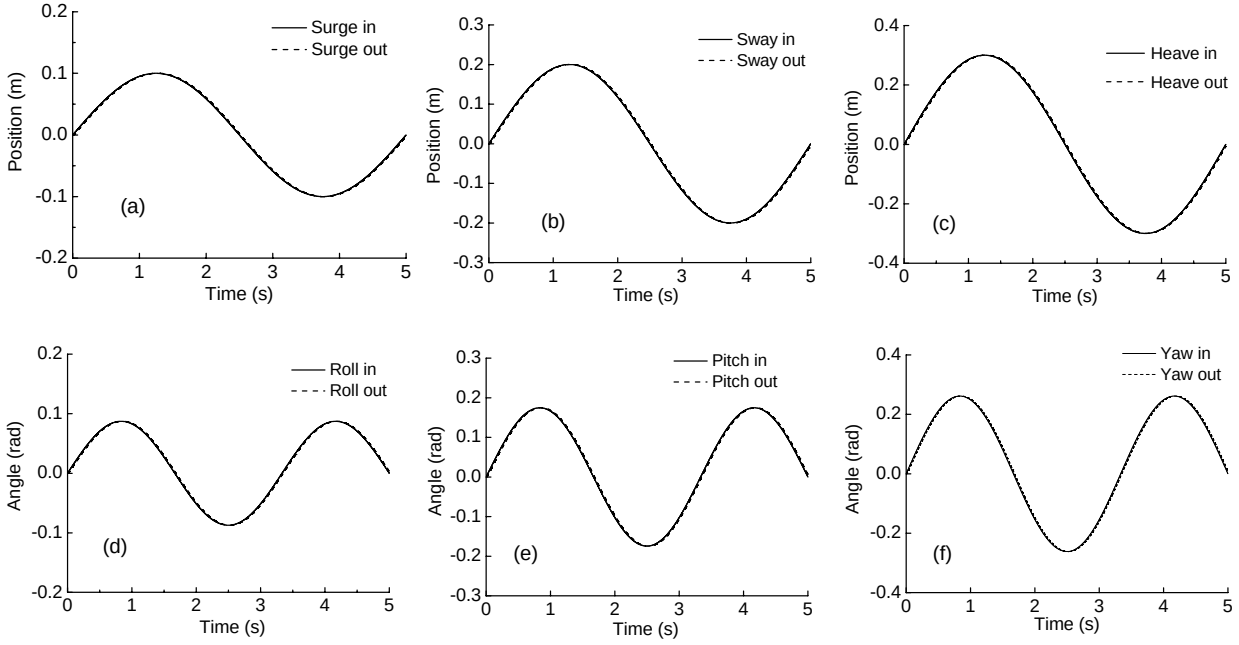

Fig. 7 Simulation results for surge (a), sway (b), heave (c), roll (d), pitch (e), and yaw (f) tracking

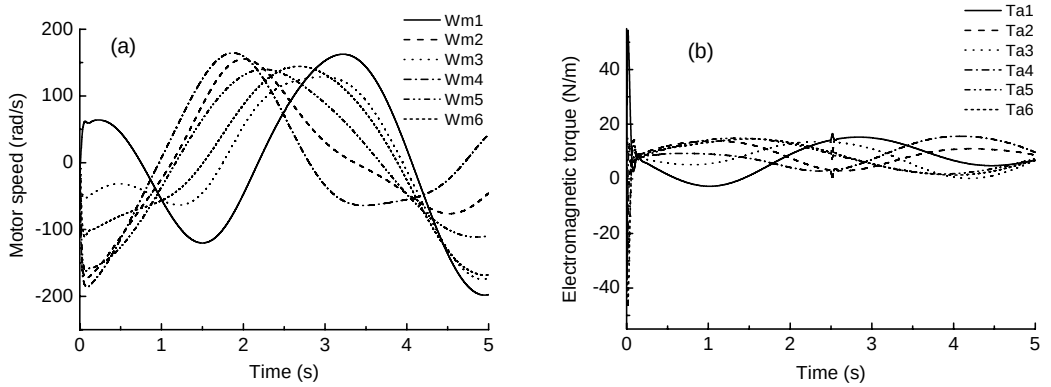

Fig. 8 Simulation results for motor speed (a) and electromagnetic torque (b)

Wm*i* (*i*=1, 2, …, 6) represents the motor speed of the *i*th actuator, and Ta*i* (*i*=1, 2, …, 6) represents the electromagnetic torque of the *i*th actuator

In Fig. 7, the Stewart platform can achieve a good position tracking of the desired trajectories, and the error of each DOF can be acceptable. In Fig. 8a, the motor speeds can quickly reach the required value at the beginning and track the input command smoothly. In Fig. 8b, the motor electromagnetic torques have some shocks and overshoots at the beginning only, and can be stabilized in about 0.15 s.

Though the external impact load is forced on the movable platform at 2.5 s to 2.7 s, the position tracking and the motor speeds do not change at all. Only the electromagnetic torques have some shocks, and these can be stabilized in a short time. Therefore, the Stewart platform is robust to external load.

To analyze the influence of the actuator inertial forces and the motor systems' mechanical movements, three single surge position commands with equal amplitude, but varied frequency, are implemented to the Stewart platform, as shown in Eqs. (37)–(39). The actual torque and the torque without the influence are as shown in Fig. 9.

The Cartesian desired trajectories of the platform are assumed to be

$$\text{Surge}: \chi_1 = 0.01\sin(2\pi t)\ \text{m}, \tag{37}$$

$$\text{Surge}: \chi_1 = 0.01\sin(4\pi t)\ \text{m}, \tag{38}$$

$$\text{Surge}: \chi_1 = 0.01\sin(6\pi t)\ \text{m}. \tag{39}$$

Fig. 9 shows that with increase in the input command's frequency, the electromagnetic torque's amplitude, the motor systems' influence ratio, and the actuators' influence ratio are wholly multiplied.

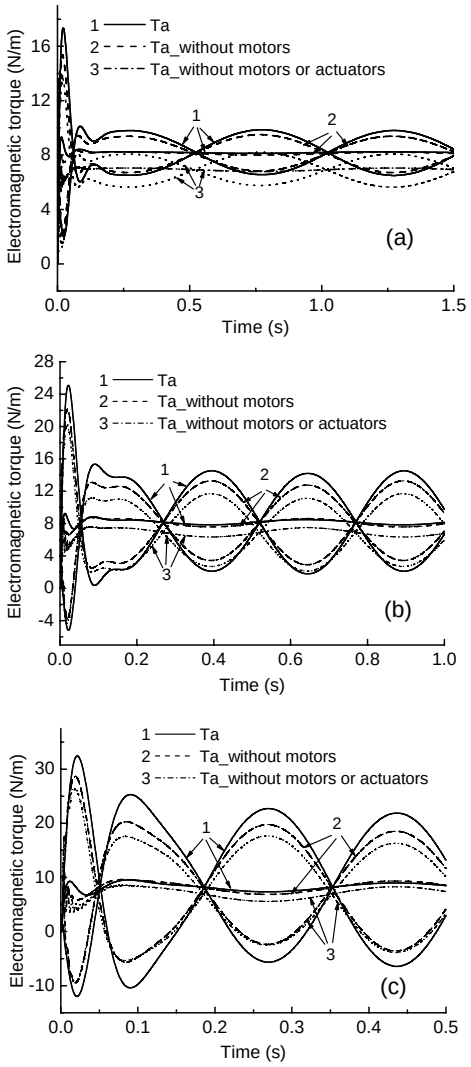

Fig. 9 Electromagnetic torque with 1 Hz (a), 2 Hz (b), and 3 Hz (c) position command

To further quantitatively analyze the influence ratios of actuators and motors, the peak-to-peak amplitude error is applied as the evaluative standard:

$$\text{error}_{\text{pp}} = \frac{|A_{T_a} - A_{T_{a\_without}}|}{|A_{T_a}|} \times 100\%, \qquad (40)$$

where A_{T_a} is the peak value of the torque T_a, and $A_{T_{a\_without}}$ is the peak value of the torque $T_{a\_without}$.

By varying the amplitude and frequency of the input command, we can list the calculation results as in Table 5.

Table 5 The influence ratios of the actuators and the motors

Simulation	Desired trajectory	Ratio_1 (%)	Ratio_2 (%)
1	$\chi_1 = 0.01\sin(2\pi t)$ m	4.0	16.1
2	$\chi_1 = 0.01\sin(4\pi t)$ m	8.8	19.9
3	$\chi_1 = 0.01\sin(6\pi t)$ m	13.2	22.9
4	$\chi_1 = 0.1\sin(0.3\pi t)$ m	3.8	17.3
5	$\chi_1 = 0.1\sin(0.6\pi t)$ m	8.2	20.1
6	$\chi_1 = 0.025\sin(2\pi t)$ m	6.0	20.0
7	$\chi_1 = 0.3\sin(0.1\pi t)$ m	2.3	16.2
8	$\chi_1 = 0.3\sin(0.2\pi t)$ m	3.2	16.4

Ratio_1: the ratio of motor systems dynamics to Stewart platform dynamics; Ratio_2: the ratio of actuators and motor systems dynamics to Stewart platform dynamics

Due to the limitations in the motor speed, the motor current, and the actuator length, the input command of the Stewart platform must be feasible, which means a low amplitude command can have a high frequency, but a high amplitude command must be of low frequency.

In Table 5, simulations 1–3, 4, 5, 7, and 8 show that Ratio_1 increases as the input command's frequency multiplies. Moreover, simulation 3 shows that Ratio_1 can be up to 13.2%. Comparing simulations 1 and 6, we can see that the amplitude's increase also leads to the increase of Ratio_1. All simulations show that Ratio_2 is within the range of 15%–23%.

In addition, Ratio_1 is much higher in high frequency and low amplitude maneuver than in low frequency and high amplitude maneuver.

Therefore, the influence of the motor systems and the actuator inertial forces cannot be ignored.

The simulation shows that the PID controller can be used in the development of an electrical Stewart platform, despite the fact that the PMSM system works under the condition of parameter variations and external load disturbances.

Using the model, we can also obtain a series of curves of the actuators position, actuators speed, motor current, rotor velocity, rotor angular tracking, and so forth. Therefore, the proposed model can be used to analyze the real system.

6 Conclusions

The development of a novel dynamics modeling of a PMSM driven 6-DOF Stewart platform was studied. Not only was the calculation of time-varying equivalent inertia avoided, but also the influence of motor system mechanical movements, counter EMF and motor friction was considered. Finally, simulations with typical desired trajectory inputs were conducted and the performance of the Stewart platform was obtained. The proposed methodology can be extended to electrical serial or closed-chain manipulators and simulators.

Numerical simulations show that, under specific conditions, the influence of motor system mechanical movements can be up to 13.2% and the influence of actuator inertial forces can be up to 14% (20%−6%). Therefore, the effect of motor systems cannot be considered negligible, especially in high frequency and low amplitude maneuvers. In addition, under the PID control, the Stewart platform is robust to the disturbance of the external load and has a good dynamic response with the bandwidths up to 10 Hz.

References

Chen, B.S., 2006. Electric Drive Control System. Mechanical Industry Press, Beijing, China, p.53-254 (in Chinese).

Chen, L., Deng, Z.Q., Yan, Y.G., 2004. Design of current control loop for permanent magnet synchronous servo system. *J. Nanjing Univ. Aeronaut. Astronaut.*, **36**(2):220-225 (in Chinese).

Dasgupta, B., Choudhury, P., 1999. A general strategy based on the Newton-Euler approach for the dynamic formulation of parallel manipulators. *Mech. Mach. Theory*, **34**(6): 801-824. [doi:10.1016/S0094-114X(98)00081-0]

Dasgupta, B., Mruthyunjaya, T.S., 1998. A Newton-Euler formulation for the inverse dynamics of the Stewart platform manipulator. *Mech. Mach. Theory*, **33**(8):1135-1152. [doi:10.1016/S0094-114X(97)00118-3]

Elmas, C., Ustun, O., Sayan, H.H., 2008. A neuro-fuzzy controller for speed control of a permanent magnet synchronous motor drive. *Exp. Syst. Appl.*, **34**(1):657-664. [doi:10.1016/j.eswa.2006.10.002]

Fichter, E.F., 1986. A Stewart platform-based manipulator general theory and practical construction. *Int. J. Robot. Res.*, **5**(2):157-182. [doi:10.1177/027836498600500216]

Fu, S.W., Yao, Y., Wu, Y.Q., 2007. Comments on "A Newton-Euler formulation for the inverse dynamics of the Stewart platform manipulator" by B. Dasgupta and T.S. Mruthyunjaya. *Mech. Mach. Theory*, **42**(12):1668-1671. [doi:10.1016/j.mechmachtheory.2006.01.010]

Gao, X.S., Lei, D.L., Liao, Q.Z., Zhang, G.F., 2005. Generalized Stewart-Gough platforms and their direct kinematics. *IEEE Trans. Robot.*, **21**(2):141-151. [doi:10.1109/TRO.2004.835456]

Geng, Z., Haynes, L.S., Lee, J.D., Carroll, R.L., 1992. On the dynamic model and kinematic analysis of a class of Stewart platforms. *Robot. Autonom. Syst.*, **9**(4):237-254. [doi:10.1016/0921-8890(92)90041-V]

Gough, V.E., 1956. Contribution to discussion of papers on research in automobile stability, control and tyre performance. *Proc. Auto Div. Inst. Mech. Eng.*, p.392-394.

Jan, R.M., Tseng, C.S., Liu, R.J., 2008. Robust PID control design for permanent magnet synchronous motor: a genetic approach. *Electr. Power Syst. Res.*, **78**(7):1161-1168. [doi:10.1016/j.epsr.2007.09.011]

Ji, Z., 1993. Study of the Effect of Leg Inertia in Stewart Platforms. Int. Conf. on Robotics and Automation, **1**:121-126. [doi:10.1109/ROBOT.1993.291971]

Kang, C.G., 2001. Closed-form force sensing of a 6-axis force transducer based on the Stewart platform. *Sens. Actuat. A*, **90**(1-2):31-37. [doi:10.1016/S0924-4247(00)00564-1]

Khalil, W., Guegan, S., 2004. Inverse and direct dynamic modeling of Gough-Stewart robots. *IEEE Trans. Robot.*, **20**(4):754-762. [doi:10.1109/TRO.2004.829473]

Kim, N.I., Lee, C.W., 1998. High Speed Tracking Control of Stewart Platform Manipulator via Enhanced Sliding Mode Control. IEEE Int. Conf. on Robotics and Automation, p.2716-2721.

Koekebakker, S.H., 2001. Model Based Control of a Flight Simulator Motion System. PhD Thesis, Delft University of Technology, the Netherlands.

Liu, M.J., Li, C.X., Li, C.N., 2000. Dynamics analysis of the Gough-Stewart platform manipulator. *IEEE Trans. Robot. Automat.*, **16**(1):94-98. [doi:10.1109/70.833196]

Omran, A., Kassem, A., El-Bayoumi, G., Bayoumi, M., 2009. Mission-based optimal control of Stewart manipulator. *Aircraft Eng. Aerospace Technol.*, **81**(3):226-233. [doi:10.1108/00022660910954736]

Shim, J.H., Park, J.Y., Kwon, D.S., Kim, S., 1997. Kinematic Design of a Six Degree-of-Freedom In-Parallel Manipulator for Probing Task. Proc. IEEE Int. Conf. on Robotics and Automation, p.2967-2973. [doi:10.1109/ROBOT.1997.606738]

Stewart, D., 1965. A Platform with Six Degrees of Freedom. Proc. Institution of Mechanical Engineers, **180**:371-386. [doi:10.1243/PIME_PROC_1965_180_029_02]

Ting, Y., Chen, Y.S., Jar, H.C., 2004. Modeling and control for a Gough-Stewart platform CNC machine. *J. Robot. Syst.*, **21**(11):609-623. [doi:10.1002/rob.20039]

Wai, R.J., 2001. Total sliding-mode controller for PM synchronous servo motor drive using recurrent fuzzy neural network. *IEEE Trans. Ind. Electron.*, **48**(5):926-944. [doi:10.1109/41.954557]

Yiu, Y.K., Cheng, H., Xiong, Z.H., Liu, G.F., Li, Z.X., 2001. On the Dynamics of Parallel Manipulators. Proc. IEEE Int. Conf. on Robotics and Automation, **4**:3766-3771. [doi:10.1109/ROBOT.2001.933204]